Competitive surface segregation of C, Al and S impurities in Fe(100)

2003 J. Phys.: Condens. Matter 15 3517

(http://iopscience.iop.org/0953-8984/15/21/302)

INSTITUTE OF PHYSICS PUBLISHING JOURNAL OF PHYSICS: CONDENSED MATTER

J. Phys.: Condens. Matter **15** (2003) 3517–3529 PII: S0953-8984(03)60545-X

Competitive surface segregation of C, Al and S impurities in Fe(100)

V Blum, A Schmidt, W Meier, L Hammer and K Heinz

Lehrstuhl für Festkörperphysik, Universität Erlangen-Nürnberg, Staudtstraße 7, D-91058 Erlangen, Germany

E-mail: kheinz@fkp.physik.uni-erlangen.de

Received 6 March 2003
Published 19 May 2003
Online at stacks.iop.org/JPhysCM/15/3517

Abstract

The stoichiometries and geometric structures formed by the segregation of C, Al and S on a Fe(100) surface have been investigated by Auger electron spectroscopy and quantitative low-energy electron diffraction (LEED). Stepwise annealing of a sputtered surface with increasing annealing temperature reveals the successive segregation of C, Al and S. According to quantitative LEED analyses, each segregand forms a distinct c(2 × 2) long-range ordered structure. Also, each segregand removes the preceding one from the surface entirely, i.e. segregation in the Fe(100)–(C, Al, S) system is purely competitive with no ordered co-segregation regimes involving two or even three elements. The c(2 × 2) phases of segregated carbon and sulfur consist of elemental surface adlayers with the adatoms residing in four-fold symmetric hollow sites of the iron substrate. This is in contrast to segregated Al which, according to an earlier analysis, forms a c(2 × 2)-symmetric surface alloy layer with iron. In all cases there is some chemical disorder within subsurface layers with Fe atoms substituted by Al. The bond lengths between the segregated adatoms and iron neighbours are close to the sum of the covalent radii of the elements involved whereby carbon appears to be five-fold coordinated, in contrast to four-fold coordinated sulfur.

(Some figures in this article are in colour only in the electronic version)

1. Introduction

Segregation of the non-metallic impurities carbon and sulfur to interfaces in iron-based materials is of considerable technical importance, in particular as it affects material properties such as the corrosion resistance or the mechanical strength of steel. Their effect can be both beneficial or detrimental: while C segregation is said to strengthen the cohesion of Fe grain boundaries, the segregation of S leads to their embrittlement (see, e.g., [1] and

references therein). Similarly, S also weakens the adhesion of protective oxide overlayers in corrosive environments [2]. Consequently, the segregation of C [3–5] and S [6–8] in pure Fe has been studied often, mostly at free surfaces because of their easier experimental accessibility. From these studies, it is clear that sulfur is by far the stronger segregand, and fully displaces the (kinetically) faster-segregating carbon from the surface in equilibrium.

Of course, the physics of segregation does not stop there—in real materials, further elements are always co-alloyed either by accident ('tramp elements') or purposely to achieve a desired effect. Hence, the influence of third elements on the Fe–C, Fe–S and Fe–(C, S) segregating systems is the subject of frequent investigation. Specifically, two possible types of behaviour are distinguished:

- Segregation of C and S in dilute Fe–Si alloys is a prototypical example for *site competition*: while Si is able to displace segregated C from a surface [9, 10] or interface [11] at elevated T, it is in turn displaced by S at yet higher T, at least for surfaces [9, 12–14] (see, for example, [15], which claims S to be displaced by Si at high T is in contrast to the remaining literature). This sequence is commonly viewed as a kinetic effect caused by different impurity diffusivities, but at least one study claims equilibrium C segregation against Si in Fe at low T [9].
- *Co-segregation* of C is reported with some added transition metals, e.g. Ti, V and Cr, resulting in ordered two-dimensional compounds on Fe surfaces [16–18]. In contrast, any potential evidence for a co-segregation of S with transition metals on (ferritic) Fe is at best weak (Ti [16], Cr [19–21]) or the segregation pattern is unclear (Mo [22, 23]).

In the present work, we address the influence of Al on the combined segregation behaviour of C and S in Fe. Although a well-studied alloying element to Fe ([24] provides references), Al has received much less attention than the aforementioned examples. In brief, it has been shown that

(i) S segregation occurs in the presence of protective Al_2O_3 on Fe–Al-based alloys [2] and

(ii) S segregates to the free surface of Fe_3Al-based polycrystals (containing 5% Cr) [25]. On the other hand, (iii) Al contents as low as 1.5% were reported to prevent S segregation to grain boundaries in Fe [26, 27]—in qualitative contradiction to (i) and (ii).

This brief overview sets the stage for the fundamental questions faced in the present work: is the segregation of Al with S and C of a competitive or co-segregating nature at Fe surfaces? And, does the presence of Al inhibit the segregation of C and/or S in any way? In the following, we answer these questions for the (100) surface of an Fe single crystal (provided by MPI für Eisenforschung, Düsseldorf). The bulk Al concentration is 3 at.%, placing the sample well within the bcc random alloy range between Fe and Al, with an unknown but non-zero bulk content of C and S. (Some earlier work of our group on this very sample concentrated on Al segregation alone, with that of C and S suppressed by suitable preparation [24].) We apply Auger electron spectroscopy (AES) to monitor the segregation behaviour of the elements for increasing annealing temperature. Our main tool is quantitative low-energy electron diffraction (LEED), allowing us to monitor the development of stoichiometrically ordered phases at the surface. The measurement and quantitative analysis of LEED intensity spectra reveals the nature of the segregand-formed structures, the layer-dependent stoichiometries within the Fe(100) surface and all atomic coordinates within the near-surface region. A recent review of similar structure determinations of bcc-type alloy surfaces can be found in [28].

2. Experimental and computational details

All measurements were performed in an ultrahigh vacuum (UHV) chamber with a base pressure of 2×10^{-11} mbar, equipped with a three-grid backview LEED optics and a hemispherical energy analyser for AES studies. An ion sputter gun was used to clean the sample prior to the different investigations (Ar ion sputtering, 2 kV, 15 μA cm^{-2}, 3 min, 100 K), whereby repeated sputtering and subsequent annealing led to a successive decrease of the carbon concentration within the surface slab. The annealing of the sputtered surface at temperatures up to about 1250 K was accomplished by electron bombardment from the sample's rear, controlled by a $WRe_{3\%}$–$WRe_{25\%}$ thermocouple attached to the sample. Fast cooling from elevated temperatures was achieved by contact with a liquid nitrogen reservoir, allowing us to reach temperatures below 100 K—at which LEED and AES data were taken—within about 2 min.

Auger signals were taken at 47 eV for Fe, at 68 eV for Al, at 152 eV for S and at 272 eV for C. The abundances of the minority elements Al, C and S were monitored by their respective peak-to-peak amplitudes normalized to that of Fe. We do not attempt to calculate the different elements' relative concentrations quantitatively. This evaluation would require the knowledge of AES cross sections and matrix factors. Yet, precise information on these is unavailable, and for safely grounded qualitative insights we prefer the raw data over a questionable extrapolation.

For more quantitative analyses, LEED intensity versus energy spectra, $I(E)$, were recorded using a fast, computer-controlled video LEED system [29, 30]. Normal incidence of the primary electron beam was adjusted by comparison of the spectra of symmetry-equivalent beams. Eventually, symmetry-equivalent spectra were averaged in order to reduce the influence of any residual misalignment and possible inhomogeneities of the luminescent screen, and to improve the signal-to-noise ratio.

For the analysis of experimental intensity spectra both full dynamical LEED calculations and the Tensor LEED perturbation method [31, 32] were applied, using the *TensErLEED* program package [33] for the latter. Optimized parameters include geometry, layer-dependent concentration of chemical species (chemical Tensor LEED [34, 35] applying the average t-matrix approximation [36]) and vibrational amplitudes of surface atoms (vibrational Tensor LEED [37]). To ensure that the validity range of the perturbation method was not exceeded during the structural search, a new reference calculation was performed whenever, after optimization, one or several parameters deviated appreciably from the preceding reference structure. The real part of the inner potential, V_{0r}, varied with energy according to the energy dependence of the exchange–correlation potential. The resulting expression, computed by Rundgren [38], is $V_{0r}(E) = V_{00} - \max[(0.24 - 72.98)/\sqrt{(E/\mathrm{eV} + 6.76)}; -10.30]$ eV, whereby the unknown part V_{00} was adjusted in the course of the theory–experiment fit. The imaginary part of the inner potential, which simulates the electron attenuation, was set constant, $V_{0i} = 5$ eV. The atomic scattering for energies up to 500 eV was described by up to 13 fully relativistic and spin-averaged phase shifts.

An automated structural search procedure [39] was applied for the search for the best fit in the multi-dimensional parameter space, guided by the Pendry R factor [40] for the quantitative comparison of experimental and computed spectra. Error limits for the various parameters were estimated by the variance of the R factor, $\mathrm{var}(R) = R_{min}\sqrt{8V_{0i}/\Delta E}$, with R_{min} the minimum R factor and ΔE the energy width of the beam accumulated database [40]. Possible correlations between different parameters are neglected in the conventional error estimate.

3. Qualitative features resulting from AES and LEED

In order to follow the segregation process by AES, the freshly sputtered crystal surface (with its carbon content already reduced by prior sputtering) was annealed in steps of increasing

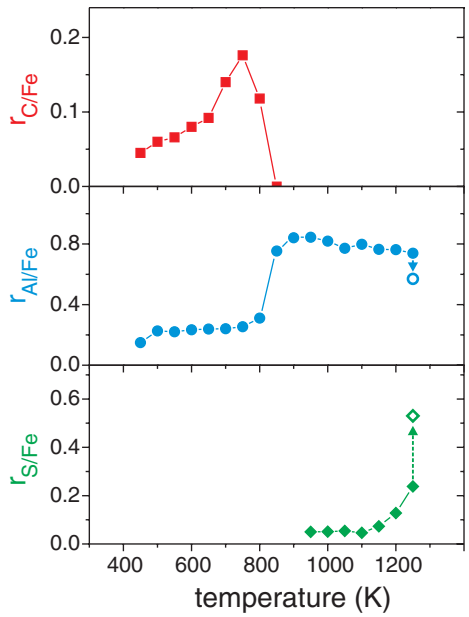

Figure 1. AES peak-to-peak signals of C (top), Al (middle) and S (bottom) relative to that of Fe as a function of annealing temperature. At each temperature point the annealing time was 5 min except for the last two points for Al and S indicated by arrows where an extra annealing of 20 min was applied.

temperature. After each step, the sample was quenched to below 100 K for AES data acquisition and LEED pattern observation.

The Auger spectrum of the freshly sputtered surface shows only small or even undetectable amounts of C, Al and S. With progressive annealing in steps of 50 K the signals increase by surface segregation. Figure 1 displays the ratio $r^{\mathrm{AES}}_{\mathrm{X/Fe}}$ of the peak-to-peak amplitudes of the three elements X = C, Al, S relative to the Fe signal with increasing T. The annealing time at each temperature point was 5 min. At 1250 K the sample was additionally annealed for another 20 min as indicated by arrows and open symbols. This caused a further increase of the sulfur signal paralleled by a decrease of the Al signal and led to the formation of clear c(2×2) superstructures (in contrast, the same extra annealing at 700 K hardly changed the C and Al signals). The decrease of the C signal above 700 K is accompanied by the growth of the Al signal, which in turn saturates above about 850 K. In contrast to $r^{\mathrm{AES}}_{\mathrm{C/Fe}}$, a decrease of $r^{\mathrm{AES}}_{\mathrm{Al/Fe}}$ does not follow immediately; instead, the saturation level is approximately retained up to 1200 K, where it starts to drop, in particular by prolonged annealing. Segregation of S is only observed above 1100 K, encountering a steep increase as the Al concentration drops. Note that a further increase of the annealing temperature above 1250 K had to be avoided because Al starts to evaporate from the surface.

As mentioned in section 2, the signal strengths of S, C and Al *relative to one another* are somewhat arbitrary, since their conversion to surface concentrations was not attempted. Still, it is qualitatively clear that surface segregating Al forces already segregated C back into the bulk, i.e. competitive segregation is observed. The drop of Al with beginning S segregation indicates the same for these two elements, particularly the continued decrease in the Al signal with prolonged annealing time (highest T in figure 1). However, S and Al still coexist clearly even at 1250 K, so that some co-segregation between both is not ruled out by AES—the answer is left up to the LEED analysis.

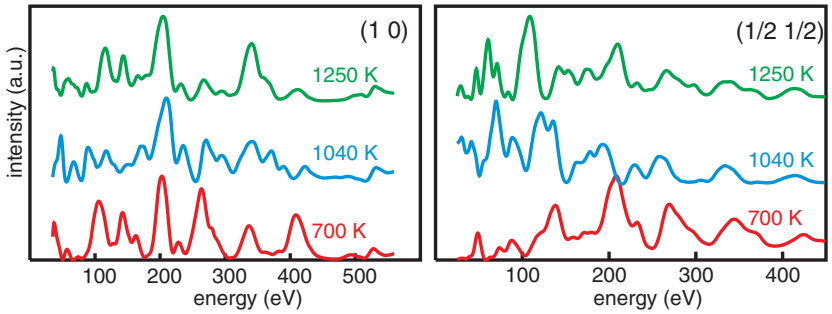

Figure 2. LEED $I(E)$ spectra for selected beams of the three c(2 × 2) phases developed for the maximum segregation of C, Al and S as represented by the annealing temperatures given (see figure 1).

When the Auger signals of the three elements reach their maximum the LEED pattern is always of c(2 × 2) symmetry. For the ordered phases, $I(E)$ spectra were recorded after prolonged annealing (for about 20 min) at 700 K (c(2 × 2)-C), 1040 K (c(2 × 2)-Al) and 1250 K (c(2 × 2)-S), and after quenching the sample to about 100 K in each case. In spite of the same c(2 × 2) symmetry of the phases, the underlying atomic structures must be different, as evident from the rather different $I(E)$ spectra. They are compared to each other for a selected integer- and half-order beam in figure 2. The data taken at 1040 K, i.e. for dominating Al segregation, are identical to those of the c(2 × 2) phase observed earlier for a specially prepared, impurity-depleted $Fe_{97}Al_{03}(100)$ surface [24]. This phase has been quantitatively analysed by LEED within the same work, with the main result that in the top layer of the surface half of the Fe atoms are substituted by Al so that a chemical c(2 × 2) superstructure is formed. This single-layer alloy is buckled, i.e. the centres of the Al atoms are displaced outwards by 0.06 Å relative to the plane made up by the Fe atoms [24]. Except for some minor concentration in the third layer, no Al enrichment is found in deeper layers.

The principal 'LEED question' in the present work will be to determine the sites taken by surface-segregated C and S. Particular attention must be paid to any possible correlation between S/C site occupancy and that of Al, to decide whether or not a co-segregation effect can be attested. As indicated by the Auger signals, no co-segregated sulfur is expected for the c(2 × 2)-C phase. However, some surface enrichment in Al should at least be tested for in the analysis. Vice versa, no carbon is expected in the c(2 × 2)-S phase. Given the significant decrease of $r^{\mathrm{AES}}_{\mathrm{Al/Fe}}$ in the last (prolonged) annealing step, its equilibrium presence in the c(2 × 2)-S phase is rather uncertain, but not ruled out by AES—only the LEED analysis can settle this point. Before starting, we recall at this point that—according to our earlier work [24, 41]—the c(2 × 2) phase developing upon Al segregation consists of a Fe/Al chemical superstructure, i.e. an atomic adlayer with Fe and Al atoms arranged according to the c(2 × 2) symmetry. The adlayer itself is nearly perfect for this structure, with less than 10% defects in the adlayer estimated both from quantitative LEED and the ratios of experimental and calculated energy averaged intensities of fractional- and integer-order LEED spots [41]. A slight subsurface Al enrichment is possible but within the error limits of the analysis.

4. Surface structure of the c(2 × 2)-C phase

The database of the c(2 × 2)-C phase consists of spectra for three fractional-order spots with a cumulative energy width of $\Delta E_f = 850$ eV and eight integer-order spots with $\Delta E_i = 2045$ eV,

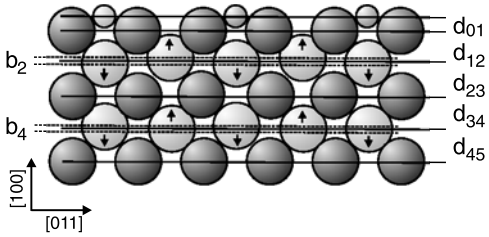

Figure 3. Structural model of c(2 × 2)-C/Fe(100) with C atoms residing in four-fold hollow sites.

so that the total energy width amounts to $\Delta E = 2895$ eV. In a preliminary structural search full dynamical calculations were carried out for four qualitatively distinct models:

(i) For the model of substitutional segregation—as found for the Al-segregated surface—the achievable R factor was only $R \approx 0.7$, so that this model could be ruled out safely. Alternatively, we tested adsorption models with C residing in
(ii) hollow,
(iii) bridge and
(iv) top sites.

Of these the hollow site model (ii) produced by far the best agreement (preliminary result: $R = 0.2$; in contrast, $R = 0.6$ for models (iii) and (iv)). So, an extensive structural search was performed for this model, using the Tensor LEED approach to handle the considerable number of parameters to be tested. The geometrical parameters are visualized in figure 3. The adsorption height d_{01} and first four substrate interlayer spacings were allowed to vary, together with an adsorbate-induced buckling of the second and fourth substrate layers (with the sign of the movement indicated by arrows). The interlayer spacings d_{ik} are measured with respect to the centre of mass planes of the different layers. On the chemical side, we allowed for statistical vacancies in the adlayer (described by the C concentration c_0(C)). Also, statistical substitutions of Fe atoms by Al in the first substrate layer (described by c_1(Al)) as well as in the second substrate layer were considered. In the latter we differentiated between sites vertically below the adatom (described by c_{21}(Al)) and the remaining sites (described by c_{22}(Al)). Finally, isotropic atomic vibrations in the adsorbate layer (amplitude v_0), the first substrate layer (v_1) and the two sites of the second substrate layer (v_{21}, v_{22}) were accounted for. The vibrational amplitude of deeper layer atoms was held fixed at $v_b = 0.07$ Å given by the Debye temperature of bulk Fe. So, the total number of geometrical, chemical and vibrational parameters is $N = 15$. Given that any peak in an $I(E)$ spectrum with a total width of about $4V_{0i} \approx 20$ eV provides independent structural information, we need a database width of $20N = 300$ eV at minimum. With $\Delta E = 2895$ eV available the redundancy factor is larger than 9 so that the analysis is statistically sound.

The structural search resulted in a best fit quantified by a Pendry R factor of $R_{min} = 0.118$, with about the same level achieved for the subsets of integer- and half-order beam data. This is a rather convincing level of agreement between experimental and calculated model intensities. The visual comparison is equally favourable, demonstrated for some selected beams in figure 4. The numerical values of the best-fit parameters are summarized in table 1, together with the bond length of C to the top and second layer Fe atoms calculated from the adsorption height.

The structural result will be discussed in section 6 together with that for the c(2 × 2)-S/Fe(100) phase presented in the next section. At this point we only address the

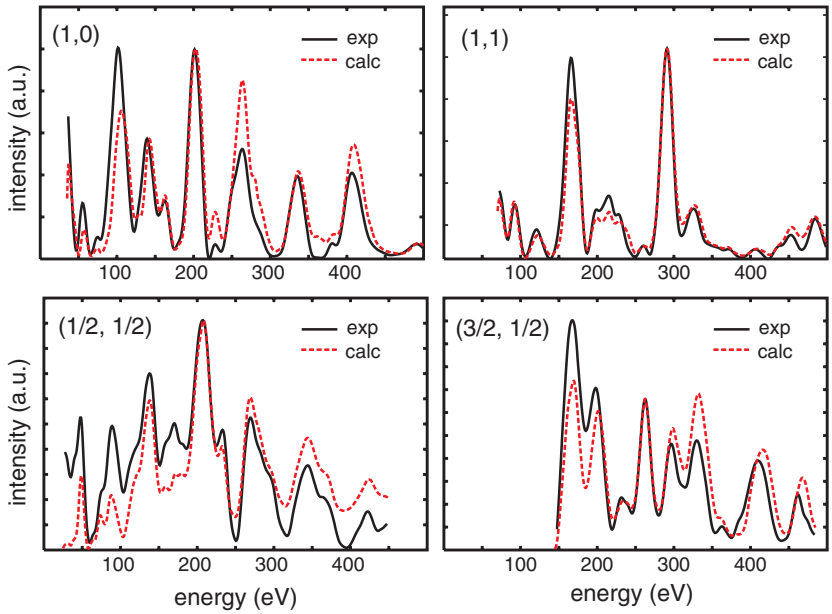

Figure 4. Comparison of experimental spectra (full curves) and calculated best-fit data (broken curves) of the C(2×2)-C/Fe(100) phase for some selected beams.

issue of errors. Their calculation for single parameters (i.e. neglecting parameter correlations) from the R-factor variance, $\mathrm{var}(R) = 0.014$, yields about ± 0.05 Å for the carbon adsorption height and ± 0.01 Å for substrate interlayer spacings and layer bucklings (the increased value for carbon is due to its comparatively weak scattering strength). In the best-fit structure there are no carbon vacancies in the adlayer at all (within the single-parameter error $\pm 5\%$ for c_0). However, the error for the C vibrational amplitude v_0 is as high as 0.08 Å. In fact, c_0 and v_0 are correlated quantities, with considerably larger combined error limits: a smaller C concentration, i.e. higher vacancy concentration, can be approximately simulated by a smaller vibration amplitude of C atoms and vice versa. So there is no safe conclusion for c_0 and v_0 from the R factor fit alone. However, a reduced C concentration, i.e. an incomplete c(2×2) adlayer, is indicated by the ratio of the energy averaged intensities of fractional- and integer-order spots, $r = \langle I_f \rangle / \langle I_i \rangle$. The value calculated for ideal order is $r_{calc} = 0.97$ whilst the experimental value is only $r_{exp} = 0.43$. This is indicative for a substantial concentration of vacancies in the adlayer; on the other hand, any local disorder (in particular due to the low annealing temperature applied) also reduces r, making it difficult to conclude a definite value for c_0. So there is some uncertainty left and we need to point out that, for an incomplete carbon adlayer, the geometrical parameters derived are average values, i.e. weighted averages with respect to occupied and unoccupied hollow sites. Equivalently, this can also be taken into account by error limits considerably larger than those given above.

5. Surface structure of the c(2×2)-S phase

Regarding the models to be tested for the c(2×2)-S phase we profit from the fact that a quantitative LEED analysis [42] and an angle-resolved photoemission fine structure (ARPEFS) study [43] are available for the adsorption phase of S on the (100) surface of a pure Fe crystal

Table 1. Results for the c(2 × 2)-C/Fe(100) phase according to the parameters defined in figure 3 and the text. $L_{\mathrm{C-Fe}1,2}$ denote the bond lengths of C to first and second layer Fe atoms. The bulk interlayer spacing in Fe(100) is $d_b = 1.433$ Å.

d_{01} (Å)	d_{12} (Å)	d_{23} (Å)	d_{34} (Å)	d_{45} (Å)	b_2 (Å)	b_4 (Å)	$L_{\mathrm{C-Fe}1}$ (Å)	$L_{\mathrm{C-Fe}2}$ (Å)
0.34	1.54	1.42	1.44	1.43	0.13	0.01	2.05	1.94
c_0(C)	c_1(Al)	c_{21}(Al)	c_{22}(Al)	v_0 (Å)	v_1 (Å)	v_{21} (Å)	v_{22} (Å)	
95%	10%	10%	0%	0.17	0.13	0.09	0.09	

(i.e. without being doped with Al). In these analyses S is found to reside in four-fold hollow sites of the substrate, i.e. there is a simple sulfur adlayer of c(2 × 2) symmetry with no surface alloying involved. So we could safely assume that this also holds in the present case if Al were not involved in sulfur bonding. Yet, in view of the still rather high Auger signal for Al it might be possible that the sulfur atoms bind to aluminium atoms, so forming some kind of co-segregation layer. Therefore, the models tested were an adlayer consisting of

- both S and Al in hollow sites and arranged to form a chemical c(2 × 2) superstructure,
- only S in surface hollow sites and the first or second substrate layer made up fully by Al atoms,
- only S in surface hollow sites and bulk-like substitutional disorder in the Fe–Al substrate (which in view of only 3% Al is close to the above-mentioned case of S on pure Fe),
- only S in surface hollow sites but with an additional chemical c(2 × 2) superstructure of Fe and Al in the second substrate layer, and
- S in bridge and atop sites was tested.

In the preliminary full dynamical calculations for these models the adsorption height, the first two interlayer spacings in the substrate and the buckling induced in the second substrate layer were varied. A database consisting of spectra for three fractional-order spots ($\Delta E_f = 1125$ eV) and eight integer-order spots ($\Delta E_i = 2070$ eV) was used, so that the total energy width amounts to $\Delta E = 3195$ eV. Only model (iii) produced a promising R factor for further structural refinement ($R = 0.17$) whilst the values for all other models were considerably higher.

Since model (iii) is symmetry-equivalent to the best fit obtained for the c(2 × 2)-C surface, the same geometric (see figure 3), chemical and vibrational quantities were optimized in the Tensor LEED refinement. In particular, Al segregation in the first two substrate layers was allowed, remembering that the c(2 × 2)-S phase develops after considerable Al segregation had taken place. In the second substrate layer, we again differentiated between sites below the sulfur adatom and other sites. The only formal difference to the c(2 × 2)-C analysis regards the possible presence of vacancies in the S adlayer. For the c(2 × 2)-S phase, we possess independent information from scanning tunnelling microscopy (STM), an ideal probe for the degree of top layer order. Figure 5 shows an atomically resolved image of this surface, exhibiting a perfectly ordered c(2 × 2) arrangement. Since not a single vacancy is visible, the LEED analysis could safely assume a full c(2 × 2)-S adlayer. In total the number of model parameters to be determined amounts to $N = 14$. As the database for the c(2 × 2)-S phase is even larger than that for the c(2 × 2)-C phase, the analysis is again on statistically safe grounds.

The structural search resulted in a convincingly low best-fit R factor, $R = 0.105$, paralleled by an equally favourable optical comparison of spectra as demonstrated in figure 6 for a selection of beams. The numerical results for all adjusted parameters are summarized in table 2, together with the bond lengths of S to top and second layer Fe atoms calculated from

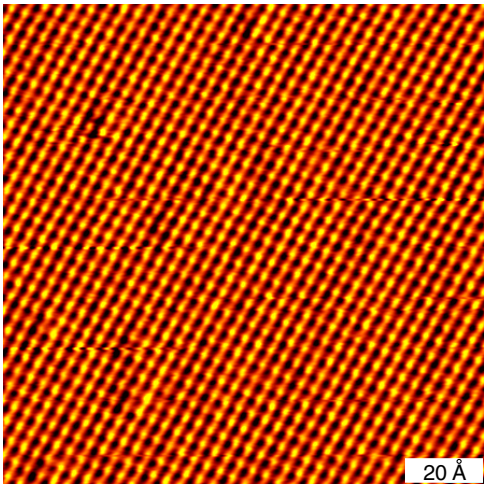

Figure 5. STM image of the c(2 × 2)-S phase (130 × 130 Å^2).

Table 2. Results for the c(2 × 2)–S/Fe(100) phase according to the parameters defined in figure 3 and the text. $L_{\text{S-Fe1,2}}$ denote the bond lengths of S to first and second layer Fe atoms. The bulk interlayer spacing in Fe(100) is $d_b = 1.433$ Å.

d_{01} (Å)	d_{12} (Å)	d_{23} (Å)	d_{34} (Å)	d_{45} (Å)	b_2 (Å)	b_4 (Å)	$L_{\text{S–Fe1}}$ (Å)	$L_{\text{S–Fe2}}$ (Å)
1.06	1.47	1.45	1.43	1.44	0.03	0.01	2.29	2.54
c_1(Al)	c_{21}(Al)	c_{22}(Al)	v_0 (Å)	v_1 (Å)	v_{21} (Å)	v_{22} (Å)		
10%	5%	0%	0.13	0.11	0.08	0.09		

the adsorption height. With an R-factor variance of var(R) = 0.012 the statistical error for the adsorption height is ±0.02 Å, considerably smaller that for the adatom in the c(2 × 2)-C phase because of the much higher scattering strength of S compared to that of C. The errors for the other interlayer spacings and the layer bucklings are of the order of ±0.01 Å. Those for the Al concentrations are of the order of ±10%, so that we cannot conclude safely that there is any Al at all left within the surface after S has segregated to it. The ratios of experimental and calculated energy averaged intensities of fractional- and integer-order spots are very close, namely $r_{exp} = 0.51$ and $r_{calc} = 0.57$. This is the LEED expression for the perfect order consistent with and obvious from the STM image presented above.

Yet, the small concentration (or even absence) of Al within the surface as obtained by LEED seems to be at variance with the Auger data (figure 1). The latter indicates that, though the Al concentration decreases with S segregation, a detectable amount of it still exists within the surface. This discrepancy can be resolved by the LEED beam intensities being sensitive only to geometrically ordered areas whilst AES is largely independent of order. In this light we conclude that there must be geometrically disordered surface patches enriched by Al which possibly are due to kinetic effects according to which the surface is not yet in full equilibrium. In LEED they cause only some background intensity which, however, is of a low level as it is distributed over the whole LEED screen (leaving diffraction spot widths unaffected). Even more, the background intensity mentioned is subtracted in the beam intensity measurement [29, 30]. As a consequence, the background has no influence on the determination of vibrational amplitudes, as those come by a fit to the beam intensities only.

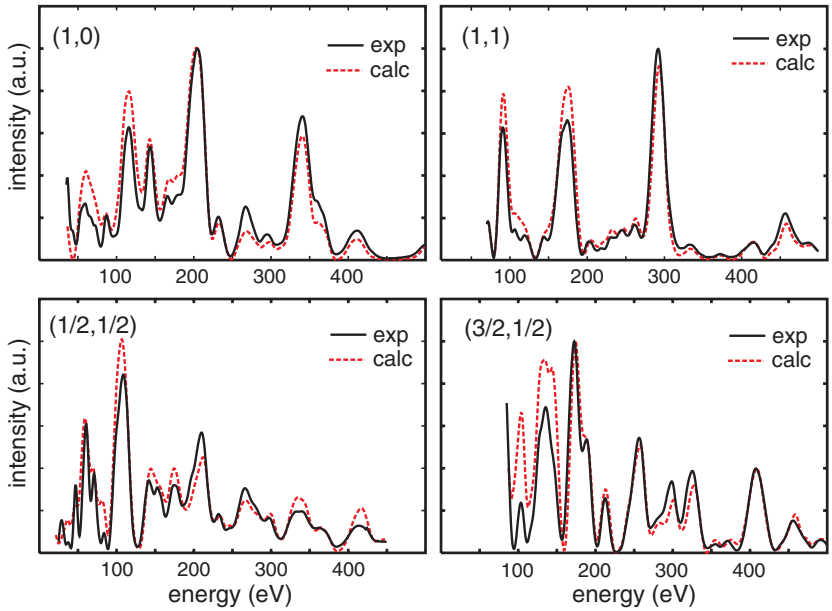

Figure 6. Comparison of experimental spectra (full curves) and calculated best-fit data (broken curves) of the c(2 × 2)-S/Fe(100) phase for some selected beams.

6. Discussion and conclusion

The excellent quality of the theory–experiment fit for the two structures determined leaves no doubt about the stoichiometry of the ordered c(2 × 2)-C(S) segregation phases. An almost defect-free substitutional occupation of top layer sites was observed earlier for the c(2 × 2)-Al phase [24].

6.1. Segregation geometry

Both carbon and sulfur segregate to the very surface and eventually reside there as adlayers occupying four-fold symmetric hollow sites in c(2 × 2) long-range order. The latter is practically perfect for c(2 × 2)-S, whilst carbon vacancies may exist in the c(2 × 2)-C phase. Because of their size, carbon atoms reside deeper within the hollow site than sulfur atoms. The carbon bond length to the top layer Fe atoms, $L_{\mathrm{C–Fe1}} = 2.05$ Å, is slightly larger than the sum of the covalent radii of the elements (2.02 Å). The bond length to the second layer Fe atom, $L_{\mathrm{C–Fe1}} = 1.94$ Å, is even smaller, indicating a strong bond, i.e. the C adatom is effectively five-fold coordinated. This is different from the situation for sulfur where the spacing to the nearest second layer Fe atom is much larger (2.54 Å) than the bond length to Fe surface atoms, $L_{\mathrm{S–Fe}} = 2.29$ Å (again, close to the sum of the covalent atomic radii of 2.287 Å). So, the sulfur atoms are definitely four-fold coordinated. Not surprisingly because of this different bonding scenario for C and S, the substrate reconstruction (buckling) induced by the adatoms on the second substrate layer is substantial for the c(2 × 2)-C phase (0.13 Å) but rather weak for the c(2 × 2)-S phase (0.03 Å). The influence on the fourth substrate layer is negligible and within the limits of errors anyway.

Comparison with the results of the above cited work on the S/Fe(100) [42, 43] is very favourable. Though adsorbate-induced reconstructive atomic movements of substrate atoms

induced were not considered in these earlier works, their S–Fe bond lengths (2.28 Å [42] and 2.30 Å [43]) are practically identical or well within the limits of errors of the present result. The additional message of our analysis is that the doping of the iron crystal with aluminium has no influence on the surface geometry and stoichiometry. There is no segregation of Al atoms to alloy with the surface S atoms.

6.2. Segregation hierarchy

By combining the LEED intensity analyses with the AES results, we can draw the following conclusions:

- *A co-segregation of Al with C and/or S does not take place*. Rather, Al represents a close equivalent to Si: It replaces the initially segregated C in roughly the same temperature range as Si [9] and is itself removed from the surface by S at slightly higher T than Si [12, 14].
- *The surface segregation of S cannot be suppressed by small Al additions alone*. This is well in line with findings (i) and (ii) mentioned in the introduction. On the other hand, it contrasts with finding (iii), which claimed the suppression of S grain boundary segregation by Al. Although grain boundaries and free surfaces do not always yield equivalent behaviour [13], strong doubt is cast on (iii).
- The site competition between C/Al and Al/S is interesting since each pair resides in *different* locations at the (100) surface (substitutional versus four-fold hollow). This indirect competition must be mediated by a much stronger bond, i.e. S(C)–Fe than S(C)–Al.
- There are two qualitatively different approaches to explain the sequential segregation during a temperature ramp, such as shown in figure 1. First, this could be an *equilibrium* effect, e.g. due to changing bulk solubilities of C and S as a function of temperature. Evidence for such behaviour has been presented for Fe–(C, Si) [9, 10]. On the other hand, our entire observation could be due to a *kinetic* effect. A linear heating ramp such as ours was modelled by Eisl *et al* [44], assuming segregands with progressively higher segregation enthalpies but progressively lower *bulk* diffusivities. For the case of Fe–(Si, S), the second (kinetic) explanation is clearly established [12, 14]. The striking similarity of our curve in figure 1 with the model of Eisl *et al* suggests the same also for Fe–(C, Al, S), placing the segregation enthalpy of Al (not measured to our knowledge) between C (0.87 eV [3]) and S (1.71 eV [7]). At least for Fe–(Al, S), our last data point in figure 1 proves the relevance of kinetics beyond doubt. However, we did not investigate the behaviour of Fe–(C, Al) as a function of annealing time, so that no definitive conclusion regarding the hierarchy of the C/Al segregation enthalpies is drawn.
- The comparison of AES and LEED results shows that care must be taken when investigating a would-be co-segregation effect by AES alone (as is often done in the literature). In the *ordered* S-covered surface area, which is monitored by quantitative LEED, there is a marked absence of Al—much in contrast to the AES data (taken after short annealing steps), which indicate a considerable simultaneous presence of S and Al at 1200 K. This can only be due to large-scale disordered surface inhomogeneities—which affect AES but do not contribute to the order-sensitive LEED beam intensities—leading the casual observer to conclude some form of Al–S co-segregation. The detailed analysis of the S-segregated ordered surface regions proves atomistically and definitively that this is not the case.

7. Conclusion

We have shown that the segregation of C, Al and S to the surface of Fe(100) is competitive, but no co-segregation of elements takes place. The sequence of segregation is controlled by the segregation energy and the element segregated at the higher temperature makes the one already segregated at a lower temperature disappear from the surface. Whilst for Al segregation an ordered single-layer surface alloy is formed with Fe and Al atoms in a $c(2 \times 2)$ arrangement, the ordered surface segregation phases for C and S consist of a single adlayer of the respective element as if deposited in an adsorption experiment. The segregated C and S adatoms reside in surface hollow sites with C—because of its smaller size—much deeper in the hollow than S, so that the coordination of the adatoms to Fe are different, namely five-fold for C and four-fold for S.

Acknowledgments

This work was supported by Deutsche Forschungsgemeinschaft (DFG). We also thank Dr H Viefhaus (MPI für Eisenforschung, Düsseldorf (Germany)) for supplying the doped Fe single crystal of excellent quality.

References

[1] Suzuki S, Tanii S, Abiko K and Kimura H 1987 *Metall. Trans.* A **18** 1109
[2] Hou P Y 2001 *Mater. Sci. Forum* **369–372** 23
[3] Grabke H J, Tauber G and Viefhaus H 1975 *Scr. Metall.* **9** 1181
[4] Grabke H J, Viefhaus H and Tauber G 1978 *Arch. Eisenhuettenwes.* **49** 391
[5] Panzner G and Diekmann W 1985 *Surf. Sci.* **160** 253
[6] Grabke H J, Paulitschke W, Tauber G and Viefhaus H 1977 *Surf. Sci.* **63** 377
[7] Tauber G and Grabke H J 1978 *Ber. Bunsenges. Phys. Chem.* **82** 298
[8] Panzner G and Egert B 1984 *Surf. Sci.* **144** 651
[9] de Rugy H and Viefhaus H 1985 *Surf. Sci.* **173** 418
[10] Es-Souni M and Mosser A 1988 *Surf. Sci.* **199** 439
[11] Kim J C, Heo N H, Na J G, Woo J S and Kim G M 1998 *Scr. Mater.* **38** 1071
[12] Militzer M, Ivashchenko Y N, Krajnikov A V, Lejcek P and Wieting J 1992 *Surf. Sci.* **261** 267
[13] Leicek P, Krajnikov A V, Ivashchenko Y N, Militzer M and Adamek J 1993 *Surf. Sci.* **280** 325
[14] du Plessis J 1993 *Surf. Sci.* **287/288** 857
[15] Es-Souni M and Mosser A 1988 *Scr. Metall.* **22** 1469
[16] Dumoulin P and Guttmann M 1980 *Mater. Sci. Eng.* **42** 249
[17] Uebing C 1998 *Prog. Solid State. Chem.* **26** 155
[18] Busch B W, Uebing C and Gustafsson T 2001 *Phys. Rev.* B **64** 115427
[19] Uebing C 1990 *Surf. Sci.* **225** 97
[20] Dziakova A, Clauberg E, Uebing C and Janovec J 1999 *Surf. Rev. Lett.* **6** 389
[21] Clauberg E, Janovec J, Uebing C, Viefhaus H and Grabke H J 2000 *Appl. Surf. Sci.* **161** 35
[22] Rolland A, Montagono M M, Roussel L and Cabane J 1997 *Appl. Surf. Sci.* **108** 425
[23] Viljoen E C and Uebing C 1998 *Surf. Sci.* **410** 123
[24] Blum V, Hammer L, Meier W, Heinz K, Schmid M, Lundgren E and Varga P 2001 *Surf. Sci.* **81** 474
[25] Hou P Y, Prüßner K, Fairbrother D H, Roberts J G and Alexander K B 1999 *Scr. Mater.* **40** 241
[26] Heo N H 1996 *Met. Mater.* **2** 49
[27] Heo N H, Park C H and Na J G 1998 *Scr. Mater.* **38** 1077
[28] Heinz K and Hammer L 1999 *J. Phys.: Condens. Matter* **11** 8377
[29] Heinz K 1995 *Rep. Prog. Phys.* **58** 637
[30] Wedler H and Heinz K 1995 *Vakuum Forsch. Praxis* **7** 107
[31] Rous P J, Pendry J B, Saldin D K, Heinz K, Müller K and Bickel N 1986 *Phys. Rev. Lett.* **57** 2951
[32] Rous P J 1992 *Prog. Surf. Sci.* **39** 3
[33] Blum V and Heinz K 2001 *Comput. Phys. Commun.* **134** 392

[34] Döll R, Kottcke M and Heinz K 1993 *Phys. Rev.* B **48** 1973
[35] Heinz K, Döll R and Kottcke M 1996 *Surf. Rev. Lett.* **3** 1651
[36] Baudoing R, Gauthier Y, Lundberg M and Rundgren J 1986 *J. Phys. C: Solid State Phys.* **19** 2825
[37] Löffler U, Döll R, Heinz K and Pendry J B 1994 *Surf. Sci.* **301** 346
[38] Rundgren J 1999 private communication
[39] Kottcke M and Heinz K 1997 *Surf. Sci.* **376** 352
[40] Pendry J B 1980 *J. Phys. C: Solid State Phys.* **13** 937
[41] Blum V 2002 *On the Interplay of Surface Segregation and Bulk Order in Binary Alloys* (Aachen: Shaker)
[42] Legg K O, Jona F, Jepsen D W and Marcus P M 1977 *Surf. Sci.* **66** 25
[43] Zhang X S, Terminello L J, Kim S, Huang Z Q, Schach von Wittenau A E and Shirley D A 1988 *J. Chem. Phys.* **89** 6538
[44] Eisl M M, Reichl B M and Störi H 1995 *Surf. Sci.* **336** 377